Underwater noise from pile driving of conductor casing at a deep-water oil platform

Alexander MacGillivray[a)]
JASCO Applied Sciences, 2305-4464 Markham Street, Victoria, British Columbia Canada

(Received 9 June 2017; revised 15 December 2017; accepted 4 January 2018; published online 26 January 2018)

Underwater noise from impact pile driving of 512 -m-long conductor casings was measured at a deep-water offshore oil platform in the Santa Barbara Channel. Beamforming measurements, obtained with a vertical array, confirmed that the primary wave front generated by hammering the conductor casing was a Mach cone propagating at an angle of 17.6° below the horizontal. Analysis of the processed array data also revealed the presence of high-frequency secondary waves at angles steeper than 45° below the horizontal. These secondary waves, which appeared to be generated near the sea-surface, dominated the acoustic spectrum of the pulses at frequencies above 1 kHz. Shallow hydrophone measurements outside the Mach cone showed clear evidence of a surface shadow zone, which was caused by the strong downward directivity of the source. Although reflected waves, diffraction, and secondary waves still produced sound inside the surface shadow zone, sound levels were 10–15 dB lower in this region. Long-term hydrophone measurements showed that there was little difference (±1 dB) in mean sound levels from impact hammering of different conductors installed at the same platform over three months.
© 2018 Author(s). All article content, except where otherwise noted, is licensed under a Creative Commons Attribution (CC BY) license (http://creativecommons.org/licenses/by/4.0/).
https://doi.org/10.1121/1.5021554

[JFL] Pages: 450–459

I. INTRODUCTION

Marine impact pile driving generates high underwater sound pressures that could exceed disturbance or injury thresholds for marine wildlife.[1–3] Regulators in the United States (U.S.) and other jurisdictions typically require that operators of marine pile driving equipment establish exclusion zones around their activities, based on maximum acceptable noise exposure guidelines for marine animals.[4,5] Many noise studies have been carried out on structural piles driven near shore in shallow water, such as those associated with piers[6] and bridges.[7,8] Offshore pile driving measurements have been mainly associated with wind farm construction,[9,10] but these have also been limited to relatively shallow water depths (<50 m). Noise from pile driving in deep water, such as at offshore platforms, has been poorly studied and consequently has little historical documentation.

This article describes acoustic measurements obtained from impact hammering of conductor casing (also called drive pipe) at a deep-water offshore oil and gas platform. Beamforming on a vertical array was used to characterize the unusual sound field generated by hammering of the drive pipe in deep water. A previous study, at a near-shore location (12.5 m deep), used vertical array measurements to establish that pile driving generates conical Mach waves.[11] To the best of the author's knowledge, no prior studies have been published documenting beamforming measurements of underwater noise from deep water (>100 m) pile driving.

Conductor casings are steel pipes that extend vertically from a drill rig, through the submerged jacket structure, and into the seabed (Fig. 1). Conductor casings that are set in place by driving them into the sediment using an impact hammer are called drive pipes and are similar to conventional piles. Unlike conventional piles, however, drive pipes are not platform structural supports. Rather, their purpose is to support a drill well and ensure structural integrity of the wellbore. They are longer and have a smaller diameter than conventional monopiles used in offshore foundations. During this study, six 512 m (1680 ft) conductor casings were installed at the ExxonMobil Harmony platform from October through December 2014. The Harmony platform is in the Santa Barbara Channel, offshore California, in 365 m (1200 ft) of water.

The Santa Barbara Channel is approximately 130 km long and 30–45 km wide, located between the Channel Islands and the east-west trending coastline. The Santa Barbara basin is the prominent feature of the Channel, with sill depths of approximately 250 m and 450 m at eastern and western entrances, respectively, with shallow (ca. 60 m) inter-island passages to the south. Over 20 marine mammal species are known to exist in this area according to the National Marine Fisheries Service (NMFS) 2012 Pacific Stock Assessment Report.[12] Marine mammal species around the Harmony platform include sea lions, which are present in and out of the water around the platform jacket structure, as well as various cetaceans, including dolphins, porpoises, and gray, blue, minke, humpback, right, and killer whales. Measures taken to mitigate noise exposures during the conductor driving included suspending barrier nets from the

a)Electronic mail: alex@jasco.com

 ©Author(s) 2018.

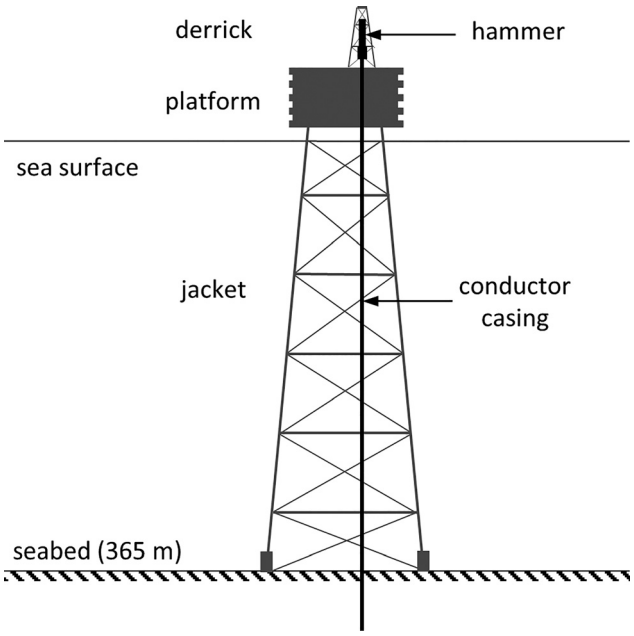

FIG. 1. Cross-section diagram of impact driving of conductor casings at the Harmony platform (not to scale). Final length of the conductor casings was 512 m and final seabed penetration was 91.4 m.

platform legs, soft starts (i.e., ramping-up the hammer when driving began), and a shut-down protocol with qualified marine mammal observers visually monitoring exclusion zones before, during, and after hammer operation.

II. DESCRIPTION OF ACTIVITY

Each of the 6 conductors (hereafter numbered 1–6) was fabricated from 42 individual pipe segments, welded together to form a steel cylinder suspended vertically from the rig floor in the water column. Each pipe segment (PSL-2 standard[13]) was 12.1 m (40 ft) long with an outer diameter of 0.66 m (26 in.), and a wall thickness of 0.025 m (1 in.). The surface of each pipe segment was coated with fusion-bonded epoxy. During construction, new segments were welded together at the rig floor as the drive pipe was lowered through the water column. At the seabed, which consisted of unconsolidated fine-grained silty-clay and clayey-silt, the conductor casings sank into the sediment under their own weight to a penetration depth of ~52 m (170 ft) below the seafloor. A hydraulic impact hammer (IHC S-90, Kinderdijk, Netherlands) drove the final four pipe segments until each conductor casing reached its final penetration depth of 91 m (300 ft) below the seafloor. A quiet period of between 1 and 8 h followed the driving of each 12.1 m segment, during which time the next segment was welded to the top of the conductor casing. The final length of each conductor casing was 512 m (1680 ft).

A Polypenco (Polyoxymethylene) cushion between the hammer and the conductor was used to dampen the impact force of the hammer. The cylindrical cushion was made of high impact plastic materials (tensile modulus of elasticity 2240 MPa, coefficient of restitution 0.904) with a thickness of 0.2 m and a diameter of 0.762 m. This cushion was removed for driving the final segment of conductor no. 1, to determine its effect on underwater sound levels. An analysis of pile driving logs from all six conductors showed that hammer energy varied approximately linearly with penetration depth ($r^2 = 0.879$), from 31 ± 7 kJ per strike at the start of driving to 59 ± 7 kJ per strike at the end of driving. The hammer repetition rate was approximately 36 strikes per minute. Between 5338 and 7554 hammer strikes per pipe were required to drive the six conductor casings to desired depth.

III. METHODS

A. Measurement apparatus

Acoustic data were collected using six JASCO Autonomous Multichannel Acoustic Recorders (AMARs; see Fig. 2). One of the AMARs incorporated a 29.75 m, eight-channel vertical hydrophone array for characterizing the directivity of the noise field generated by the conductor driving. The remaining five AMARs were single-hydrophone instruments. Table I summarizes the deployment locations, distances, and frequency ranges of the AMARs. Vertical array measurements were obtained only during driving of conductor no. 2; other hydrophones were left in place to verify that pressure signals generated by the remaining conductors were not significantly different. A vessel-based hydrophone collected additional near-surface acoustic data while conductor no. 2 was being driven.

Three AMARs (E, H, VA) were deployed on oceanographic moorings around the Harmony platform. Their on-bottom coordinates were verified to ±5 m accuracy by range-fixing their acoustic release units (Edgetech Port-LF) at four surface Global Positioning System (GPS) locations. Two AMARs (A,G) were suspended on tensioned lines inside the jacket structure, one for short-term recording (<1 week) and the other for long-term recording (3 months). One

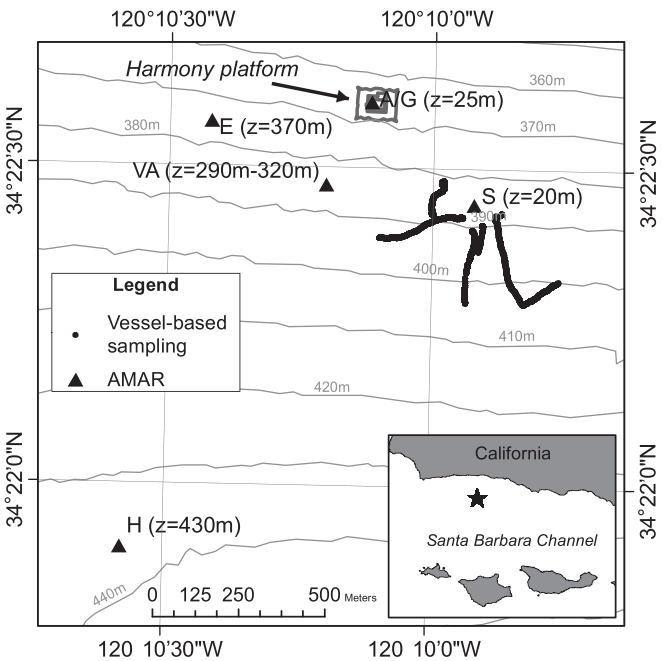

FIG. 2. Map of acoustic sensor deployment locations at the Harmony platform. Annotations indicate station name and hydrophone depth (z). Contour lines indicate water depth in 10 m increments.

TABLE I. Summary of AMAR deployment locations (NAD 83) at the Harmony platform.

AMAR	Hydrophones	Sampling rate (kHz)	Conductors recorded	Range (m)	Hydrophone depth (m)	Water depth (m)
A	1	32/365	1–6[a]	10–30	25	365
E	1	32	1	480	370	373
G	1	48	2	10	25	365
H	1	32/365	2–6	1475	430	436
S	1	48	2–3[b]	380–395	20	380
VA	8	32	2	264	290–320	372

[a]AMAR A only had a clear line of sight to the source during driving of conductor no. 2. Sound levels recorded on this sensor during driving of the other conductors were attenuated by 10–20 dB, due to shadowing by structural elements inside the platform jacket.
[b]AMAR S ran out of batteries early and stopped recording prematurely.

AMAR (S) was suspended from a heavy mooring buoy southeast of the platform; its distance varied slightly depending on prevailing currents and was periodically measured by marine mammal observers on the platform using a laser range finder.

All AMARs, including the vertical array, used omnidirectional reference hydrophones (GeoSpectrum Technologies M8K, Dartmouth, Nova Scotia, Canada) with −200 dB re 1 V/μPa nominal sensitivity. The AMARs were set to continuously record sound during the deployment period with a sampling rate of either 32 kHz or 48 kHz. Two of the AMARs (A,H) were set to record at 375 kHz sample rate on a 12% duty cycle to capture high-frequency marine mammal vocalizations (not reported in this study). Pressure waveforms were stored at 24-bit resolution on internal solid-state flash memory. Laboratory calibrations for all hydrophones were verified using a 250 Hz pistonphone (G.R.A.S. 42AC, Holte, Denmark) prior to deployment and, where possible, immediately after retrieval.

The vertical array consisted of eight M8K omnidirectional reference hydrophones, suspended in the water column. Hydrophone elements were separated by 4.25 m. The vertical array incorporated a roll-pitch-yaw (RPY) sensor (Microstrain 3DM-G, Burlington, VT), which recorded the tilt and orientation of the array. The array also incorporated two charge-temperature-depth (CTD) loggers (Star Oddi DST, Gardabaer, Iceland), which measured the depth of the array and the speed of sound in water. The CTD loggers were used to sample the sound speed profile during deployment and retrieval of the vertical array.

B. Data processing

The pressure waveform data from the AMARs were processed using JASCO's PAMlab software application. PAMlab automatically detects impact piling pulses, and for each pulse computes peak sound pressure level (PK), sound pressure level (SPL), sound exposure level (SEL), and duration, as well as 1/3-octave band levels. The duration used for calculating the SPL is based on the 90% sound exposure time window (T_{90}) of each pulse.[14] The automated pulse detector used by PAMlab is based on a Teager-Kaiser threshold detector[15] with a time step of 10 ms. Sound levels for each pulse (PK,SPL,SEL,1/3-octave SEL) were computed inside a 0.8 s window, starting 0.3 s before each detection event. Average sound levels over multiple pulses were calculated in terms of mean square sound pressure (or mean sound exposure) as appropriate. The PAMlab detections were manually reviewed after processing to remove false positives. Background noise was analyzed using PAMlab to calculate SPL and power spectral density (PSD) levels for each minute of data. PSD was computed according to Welch's method[16] using a normalized Hamming window with 50% overlap.

Delay-and-sum beamforming was applied to the eight-channel hydrophone data from the vertical array using custom software to determine the vertical directivity of the conductor driving noise. Beamforming was carried out by applying phase shifts to the hydrophone channels in the frequency domain to enhance high-frequency resolution. Phase shifts were computed as a function of beam angle using the speed of sound in water calculated from temperature and salinity data collected on the array (1485 m/s). In each beam, time-dependent signal power was calculated from the mean-square-pressure of 1-ms-long, non-overlapping time windows. Beam power and beam pressure were computed for ensemble averages of 100 pulses to enhance the signal-to-noise ratio of the beam data. The precise propagation angles of individual wave fronts were determined by time-windowing the pressure signals and using downhill simplex optimization[17] to find the beam steering angle with maximum power. Incidence angles of the wave fronts were corrected for the tilt of the array, which deviated by less than $\pm 0.5^\circ$ over the duration of the measurements.

IV. RESULTS

A. Beamforming data

Beamforming analysis was applied to the vertical array data from conductor no. 2 to determine the propagation angles of the downward and upward traveling sound waves emitted by the pipe wall (Fig. 3). Four principal wave fronts were identified in the beam power data by comparing the arrival times and incidence angles with the propagation geometry (Fig. 4): an initial wave (down-going), a toe reflection (up-going), a sea-surface reflection (down-going), and a head reflection (down-going). These four primary wave fronts, which are consistent with numerical simulations of Mach wave fronts from pile driving,[2] are identified with longitudinal stress waves traveling up and down the pipe.

The acoustic pulses from the hammering were highly repeatable and only changed gradually from pulse to pulse.

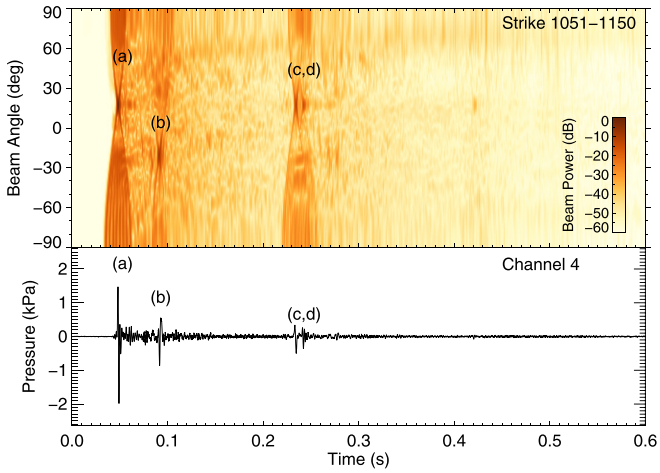

FIG. 3. (Color online) (Top) Broadband beam power versus vertical angle and time (100 strike average, normalized) showing propagation angle of primary wave fronts generated by longitudinal waves in the pipe: (a) initial wave, (b) toe reflection, (c) sea-surface reflection, (d) head reflection. Positive beam angles correspond to down-going waves, negative beam angles to up-going waves. Faint up-going seabed reflections are visible after the down-going arrivals. (Bottom) Pressure signal recorded on channel 4 of the vertical array. The hydrophone channels were assigned equal amplitude weighting while beamforming to maximize angular resolution.

The amplitude of the initial wave did not increase substantially over the duration of the conductor drive, and the per-pulse SEL remained approximately constant, despite the doubling of the hammer energy over this period (Fig. 5). Furthermore, the amplitude of the toe reflection steadily diminished over the course of the drive. This latter observation indicates that the deeper the conductor casing was driven, the more the stress wave reflection from the toe of the pipe was attenuated.

Beamforming indicated that the propagation angle of the initial wave was 17.6° (down-going) and the propagation angle of the toe reflection was −20.0° (up-going). The toe

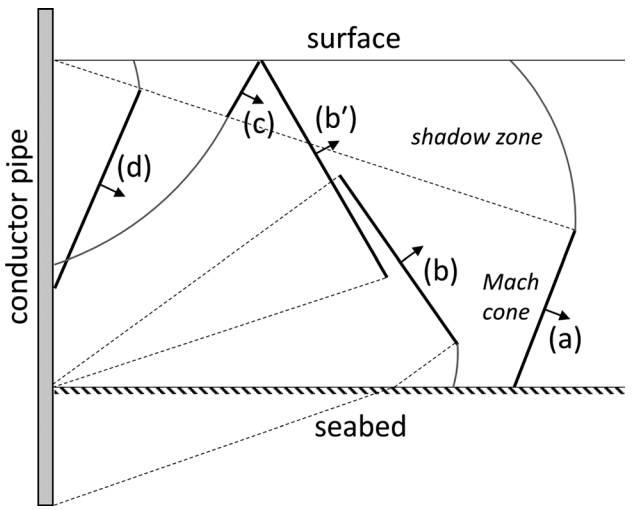

FIG. 4. Geometry of Mach cone and shadow zone inferred from vertical array data (not to scale) illustrating the four main propagation paths observed in the data: (a) initial wave, (b,b') toe reflection via sediment and water, (c) sea-surface reflection, (d) top reflection. Conical (Mach) wave fronts are represented by straight black lines, and diffracted wave fronts are represented by curved gray lines. Dashed lines follow the propagation direction of the conical wave fronts.

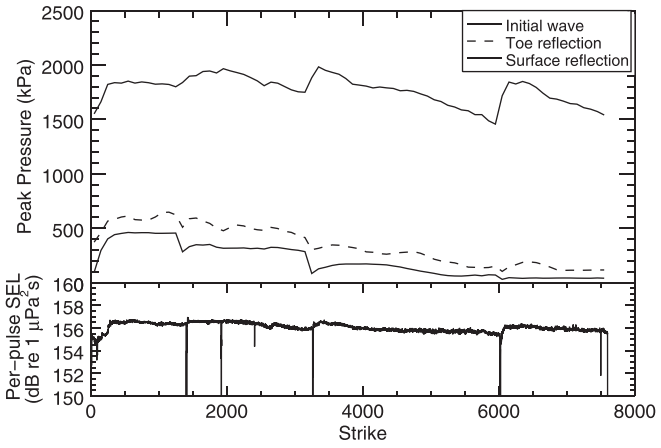

FIG. 5. (Top) Peak pressure magnitude versus strike number (100 strike average) of primary wave fronts emitted by conductor no. 2, as measured by beamforming on the vertical array. The head reflection is not shown since it could not be reliably isolated from the surface reflection. (Bottom) Per-pulse SEL versus strike number, as measured on a single channel of the vertical array during driving of conductor no. 2. Brief drops in SEL correspond to starting and stopping of the hammer and ramp-up periods.

reflection propagates at a different angle in water than the initial wave because it undergoes refraction at the seabed interface. Thus, it is possible to infer directly from the incidence angle of these wave fronts the stress wave speed in the pipe and the speed of sound in the sediments. Assuming the wave front follows a ray path from the pile wall to the receiver, and assuming a horizontally stratified ocean, Snell's law relates the grazing angle at the source (φ_s) to that of the receiver (φ_r)

$$c(z_s)/\cos(\varphi_s) = c(z_r)/\cos(\varphi_r), \tag{1}$$

where $c(z)$ is the speed of sound in the medium (water or sediment) surrounding the pipe wall, z_s is the source depth (i.e., where the ray intersects the pipe wall), and z_r is the receiver depth. The grazing angle of the Mach wave front at the pipe wall (i.e., at the source) is

$$\varphi_s = \sin^{-1}(c(z_s)/c_p), \tag{2}$$

where c_p is the speed of longitudinal stress waves in the pipe. Combining these two equations gives the following expression, which can be used to iteratively solve for the stress wave speed in the pipe and the speed of sound in the sediments:

$$\frac{c(z_s)}{c_p} = \sin\left(\cos^{-1}\left(\frac{c(z_s)}{c(z_r)}\cos\varphi_r\right)\right). \tag{3}$$

CTD measurements showed that the sound speed profile at the measurement site was downward-refracting with 1515 m/s sound speed at the sea-surface and 1485 m/s sound speed at the vertical array. The calculated longitudinal wave speed in the steel pipe was 4911 m/s, based on the propagation angle of the initial wave. This is consistent, to 2% accuracy, with longitudinal wave speeds in a steel pipe pile calculated from shallow-water beamforming measurements.[11] The calculated compressional wave speed in the top sediment layer was 1504 m/s, based on the grazing angle of

the toe reflection. The seabed sound speed estimated from the vertical array data is consistent with clayey-silt material (72% porosity),[18] which is in agreement with findings from nearby ocean drilling[19] and sediment sampling[20] surveys. This also indicates that the critical angle at the seabed (9.1°) is less than the propagation angle of the Mach cone, which is consistent with the weak seabed reflections observed in the beamforming data [the critical angle was calculated from the sound speed in water near the seabed, $c(z_b)$, and the compressional wave speed in the top sediment layer, c_b, according to $\cos^{-1}(c(z_b)/c_b)$].

A free-field measurement of the Mach wave pressure signature was isolated from the vertical array data by steering a beam at 17.6° incidence angle, windowing the first 150 ms of each pulse, and averaging the peak-aligned pressure over an ensemble of 100 pulses. The resulting signature was free of all surface and bottom reflected waves, and thus represents only the sound pressure associated with the initial down-going Mach wave (Fig. 6).

High-pass filtering revealed the presence of at least ten secondary, high-angle wave arrivals in the beamforming data (Fig. 7). The incidence angles of these secondary waves ranged from 45.6° to 57.7° (down-going), and their arrival times were clearly delayed with respect to the primary waves. Based on their incidence angles, and the location of the vertical array, these secondary waves appear to have originated close to the sea-surface, at depths less than 40 m. Their delayed arrival times and steeper incidence angles strongly suggest these secondary waves are not associated with the primary Mach cone, nor are they associated with the down-going primary stress wave in the pile.

The frequency spectra of the Mach wave and secondary waves were calculated by windowing the beamforming data over a narrow range of beam angles and arrival times (Fig. 8). This analysis showed that the transition between the two types of waves was between 1000 and 1500 Hz, with the Mach wave dominating at low frequencies and the secondary waves dominating at high frequencies. The low-frequency limit of secondary wave spectrum could not be precisely determined from the vertical array data, because the beamforming could not entirely exclude the Mach wave energy from the secondary wave spectrum below 1000 Hz.

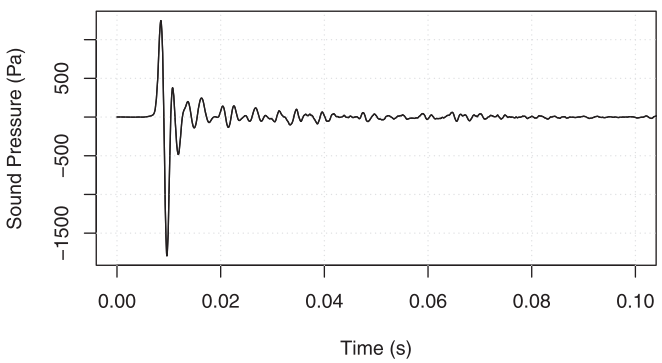

FIG. 6. Acoustic pressure signature of the down-going initial Mach wave traveling at 17.6° grazing angle, as measured on the vertical array at 264 m horizontal range from the source.

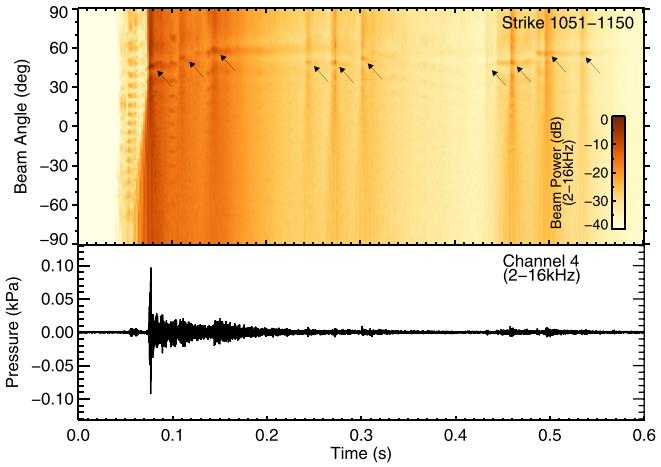

FIG. 7. (Color online) (Top) High-pass filtered (>2 kHz) beam power versus vertical angle and time (100 strike average, normalized) showing secondary high-frequency arrivals. Arrows indicate the locations of beamforming peaks corresponding to the secondary wave fronts. (Bottom) Filtered pressure signal recorded on channel 4 of the vertical array. The hydrophone channels were shaded with a Hamming window while beamforming to suppress side lobes. Filtering was applied in the frequency domain using a sixth-order, zero-phase Butterworth filter.

B. Sound levels

To analyze noise propagation away from the source, underwater sound levels were measured at 10–1475 m range during driving of conductor nos. 1 and 2. These measurements were collected into plots of sound level versus horizontal distance from the conductor (Fig. 9). Comparison of sound levels measured at different depths showed evidence of a shadow zone near the sea-surface (i.e., outside the 17.6° Mach cone). At 300–750 m range, broadband sound levels measured at 20 m depth were approximately 10–15 dB less than sound levels measured lower in the water column.

Pressure pulses recorded at the different sampling locations showed patterns of arrivals that were consistent with the four primary longitudinal wave fronts identified in the vertical array data. Inspection of the spectrograms also

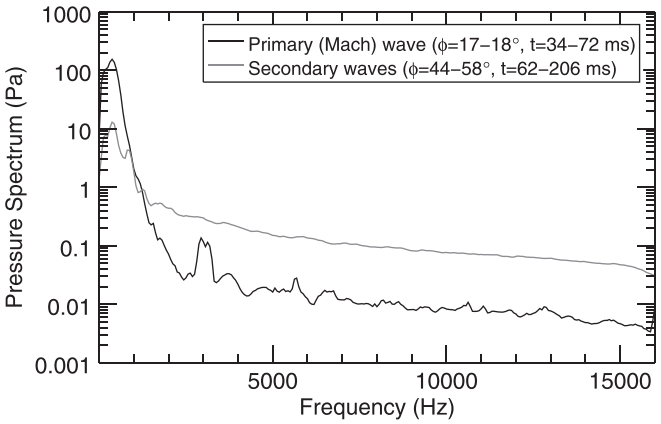

FIG. 8. Pressure spectra of the primary (Mach) wave and secondary waves (100 strike average), calculated by windowing the beamforming data and averaging over the specified range of beam angles (φ) and arrival times (t). The root-mean-square (rms)-average pressure spectrum was calculated from the beam pressure data using an advancing 512-point fast Fourier transform (FFT; 50% overlap, Hamming window). The hydrophone channels were shaded with a Hamming window while beamforming to suppress side lobes.

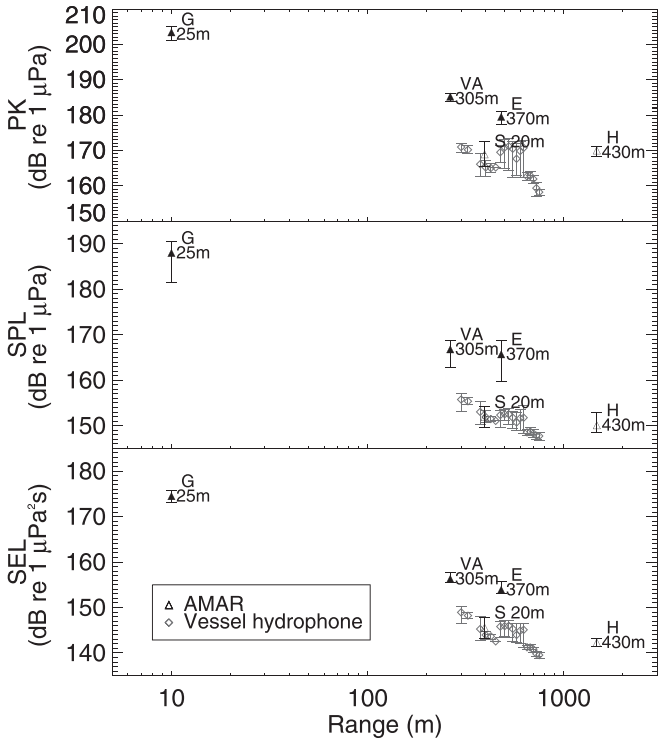

FIG. 9. PK, SPL, and per-pulse SEL versus horizontal range recorded during driving of conductor nos. 1 and 2 (with cushion). Plot annotations indicate sampling station and hydrophone depth. Error bars correspond to 90% range of sound level data. Vessel hydrophone data are shown in 25 m range bins. Filled symbols correspond to receivers inside the initial Mach cone and hollow symbols correspond to receivers inside the shadow zone.

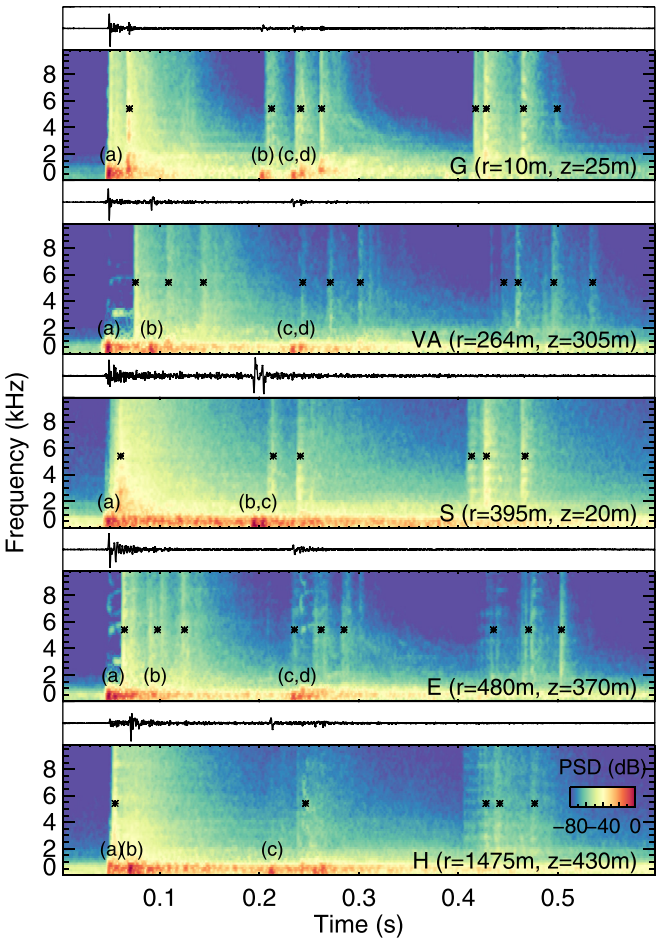

FIG. 10. (Color online) Normalized spectrograms (20 pulse average) of pulses recorded on 5 different AMARs during driving of the same pipe segment. Corresponding pressure waveforms are shown above each spectrogram. The range (r) and depth (z) of the hydrophone is indicated in the bottom right of each spectrogram. Letter annotations indicate primary arrivals generated by longitudinal waves in the pipe: (a) initial wave, (b) toe reflection, (c) sea-surface reflection, (d) top reflection. Asterisk annotations (*) indicate secondary wave arrivals, not associated with (a)–(d).

showed patterns of high-frequency arrivals corresponding to the high-angle secondary waves recorded on the vertical array (Fig. 10). These secondary waves appear to dominate the high-frequency ($\geq$1 kHz) part of the pulse spectrum.

Spectrum analysis in 1/3-octave bands was used to characterize the peak frequency of the sound energy generated by the conductor driving (Fig. 11). These measurements were obtained at sufficiently close range, and in sufficient water depth, that frequency-dependent propagation effects (e.g., multipath interference, bottom loss, absorption loss) would not have significantly affected the frequency spectrum of the sound recorded on the hydrophones. This analysis showed that pulses measured inside the primary Mach cone had lower peak frequency than those measured outside of it. Furthermore, comparing the spectrum of receivers inside the Mach cone showed that more high-frequency sound energy was received near the sea-surface than deeper in the water column.

Comparisons of long-term hydrophone measurements made outside the jacket structure showed that there was little difference ($\pm$1 dB) in mean sound levels recorded during driving of the different conductors (Table II). Thus, underwater sound levels generated by the different conductors were found to be highly repeatable at this site.

C. Effect of hammer cushion

The effect of the Polypenco cushion was examined by comparing sound levels recorded on AMAR E (inside the Mach cone) during hammering of conductor no. 1 with and without the cushion. To minimize possible bias due to changing driving conditions or hammer energy, the attenuation analysis was limited to two contiguous sets of 150 strikes recorded at the end of segment 41 (with cushion) and at the start of segment 42 (without cushion). Average sound levels with and without the cushion showed that the cushion reduced the PK by 3.3 dB, the SPL by 1.5 dB, and the per-pulse SEL by 1.8 dB. Analysis of 1/3-octave band SEL showed that the attenuation of the cushion was frequency dependent (Fig. 12). It should be noted, however, that the elastic properties of the cushion itself (and thus its effect on sound levels) may have changed over time due to frictional heating of the cushion material by the hammer. This effect could not be controlled for during the measurements due to operational constraints.

D. Back-propagation analysis

Because conical waves in free space follow a simple geometrical spreading law, measurements of the initial

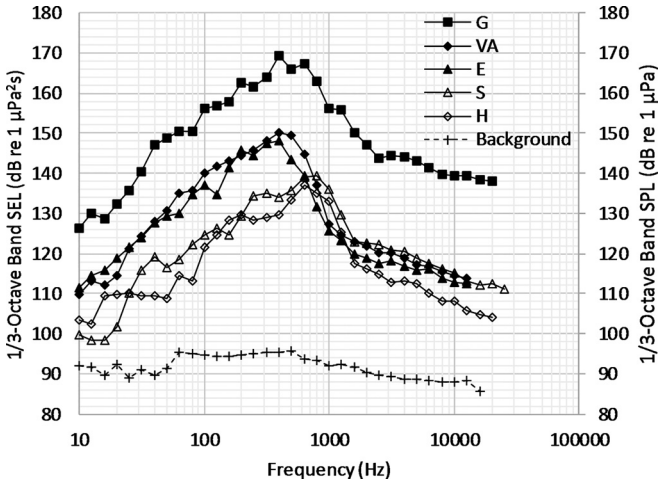

FIG. 11. Mean per-pulse 1/3-octave band SEL versus frequency at each AMAR for conductor nos. 1 and 2. Filled symbols correspond to receivers inside the Mach cone and outlined symbols correspond to receivers inside the shadow zone. Mean 1/3-octave band background noise levels (SPL, 60 s average) measured on AMAR H during periods without pile driving are also shown. While per-pulse SEL and background SPL are not directly comparable quantities, SEL is uniformly lower than the SPL for signals shorter than 1-s duration (see Fig. 9). Thus, comparing per-pulse SEL to background SPL gives a lower bound on signal-to-noise ratio for the pulses (i.e., the conductor driving was well above the background). Background noise at this location originates primarily from machinery operating on the Harmony platform.

Mach cone [wave front (a) in Fig. 4] can be back-propagated to a reference distance close to the pile. The back-propagation may be calculated using the following expression for transmission loss (TL) of conical wave fronts propagating at grazing angle φ:

$$\mathrm{TL} = 10\ \log_{10}((r/r_{\mathrm{ref}})/\cos(\varphi)), \tag{4}$$

where r is the horizontal range from the receiver point to the center of the pile, r_{ref} is the reference distance (1 m), and the quantity TL is expressed in decibels. Note that sound levels that are back-propagated according to this spreading law are not equivalent to a point source level referenced to 1 m range.

Following this approach, back-propagated sound levels, referenced to 1 m, were calculated for the Mach wave using per-pulse 1/3-octave band SEL measurements obtained inside the Mach cone on AMARs G, E, and VA (Fig. 13). Back-propagated sound levels based on conical-wave TL

TABLE II. Mean per-pulse sound levels measured outside the jacket structure, on AMARs H and S, during driving of conductor nos. 2–6. Conductor nos. 4–6 were driven after AMAR S stopped recording.

Conductor number	2	3	4	5	6
AMAR H ($r = 1475$ m)					
PK (dB re 1 μPa)	170.0	167.7	168.3	169.8	169.3
SPL (dB re 1 μPa)	150.1	148.1	148.6	150.3	149.5
SEL (dB re 1 μPa^{2}s)	142.3	141.6	141.6	143.6	142.6
AMAR S ($r = 380$–395 m)					
PK (dB re 1 μPa)	168.9	168.5	—	—	—
SPL (dB re 1 μPa)	151.9	151.7	—	—	—
SEL (dB re 1 μPa^{2}s)	145.6	145.8	—	—	—

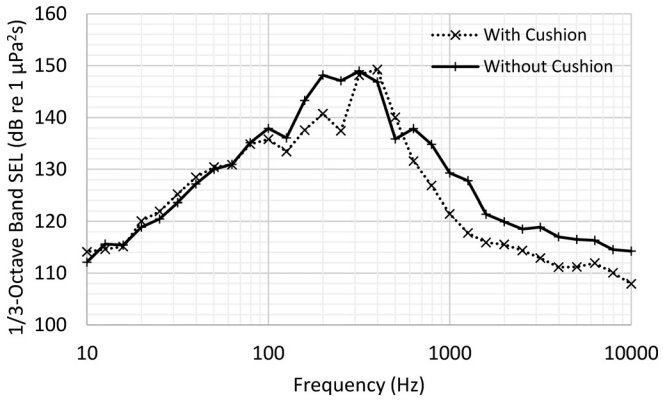

FIG. 12. Comparison of per-pulse 1/3-octave band SEL (150 strike average) with and without the hammer cushion, as measured inside the Mach cone on AMAR E.

agreed at low frequencies, but diverged above 500 Hz. Thus, for comparison, back-propagated sound levels for spherical waves ($\mathrm{TL} = 20\log_{10}(R/r_{\mathrm{ref}})$, where R is slant range) were also calculated from the same measurements under the assumption that sound from the conductor driving originated at the sea-surface. The back-propagated spherical wave sound levels agreed at frequencies above 1500 Hz (including those from AMAR S, not inside the Mach cone).

The beamforming data clearly showed that that the transition between the primary and secondary waves was between 1000 and 1500 Hz, which is higher than the upper limit of 500 Hz for the conical waves suggested by the back-propagation analysis. The explanation for this apparent difference is that the Mach wave likely decayed more rapidly with depth than cylindrical spreading would suggest above 500 Hz (another way to interpret this is that a hydrophone closer to the bottom of the pipe measured less high-frequency sound energy). Since the Mach wave was generated by a stress wave

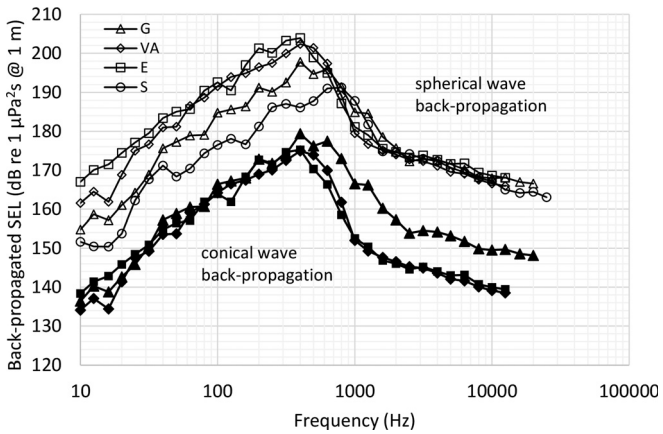

FIG. 13. Back-propagated 1/3-octave octave band SEL (per-pulse) calculated from multiple hydrophones using two different spreading laws (conical spreading and spherical spreading). Conical wave SEL values (filled symbols) were back-propagated to 1 m from the center of the pipe assuming a grazing angle of 17.6°. Spherical waves (hollow symbols) were back propagated to 1 m from the sea-surface. Only hydrophones inside the primary Mach cone were included in the conical wave back-propagation calculation. AMAR H was excluded from the back-propagation analysis because it was deemed to be too far from the source (1.5 km) to reasonably assume free-field sound propagation.

propagating down the pipe, this suggests the stress wave emitted less high-frequency sound the farther it traveled down the pipe. In a cylindrical shell, material damping and fluid loading would be expected to attenuate the sound energy radiated by stress waves in a frequency-dependent manner.[21]

Taken together, the beamforming and back-propagation results suggest that low- and high-frequency sound from conductor driving are generated by two different mechanisms: Low-frequency sound energy is generated by Mach wave radiation, distributed over the water column, whereas high-frequency sound energy is generated by localized sound radiation originating near the sea-surface. The contribution of these two different mechanisms appears to overlap in the frequency range 1000–1500 Hz. Thus, the spectrum of the sound emitted by the conductor driving appears to be depth dependent, with more high-frequency sound energy generated near the sea-surface than deeper in the water column.

V. DISCUSSION

A. Implications for assessing noise effects on marine organisms

Several results from this study are useful for assessing potential noise effects on marine life from future projects involving deep-water pile driving. One of the most important findings of this study was that receivers in the surface shadow zone were exposed to broadband sound levels that were 10–15 dB lower than receivers in the primary Mach cone. Furthermore, because the vertical extent of the shadow zone increased with distance from the source, there was an effective maximum propagation range for the primary Mach wave (estimated to be 1200 m at this site). Sound levels outside the Mach cone were influenced by site-specific properties of the substrate because reflected waves dominated received levels inside the shadow zone. Specifically, bottom loss attenuated sound waves reflected from the seabed and driving resistance attenuated stress waves reflected from the end of the conductor pipe. Thus, receivers near the sea-surface were exposed to substantially lower broadband sound levels than receivers directly in the Mach cone.

Another important finding of this study was that high-frequency secondary waves, originating near the sea-surface, dominated the high-frequency (>1 kHz) part of the sound spectrum. While these secondary waves only carried a small fraction of the broadband sound energy from the conductor driving (less than 0.3% of the total sound exposure at the vertical array), they are nonetheless important because sounds in this frequency range have the greatest potential for auditory effects on odontocetes.[22,23] Thus, when assessing potential effects of conductor driving noise on porpoise, dolphins, and other toothed whales, these secondary waves could be an important consideration.

B. Possible sources of secondary waves

It remains unclear how the high-frequency secondary waves are generated near the sea-surface. Several possible mechanisms might explain the origin of such waves:

(1) They could be generated by slower bending waves in the pipe wall.
(2) They could be sound waves reflected (or scattered) by the jacket structure.
(3) They could be refracted airborne sound waves.
(4) They could be generated by cavitation at the pipe wall.

Of these possible explanations, (1) seems most likely. Negative pressures at the pile wall are unlikely to be of sufficient intensity or duration to cause cavitation (based on SPL measured at 10 m range), and would not be expected to generate multiple waterborne arrivals. Airborne refracted waves, while possible, also do not explain the presence of multiple arrivals. Reflections of the Mach wave from the jacket structure, if present, should also have been observed in the up-going direction (they were not). Bending waves, on the other hand, are predicted by thin shell theory,[24] and travel slower than longitudinal waves in cylindrical pipes, which would explain their delayed arrival times. Different bending wave modes travel with different group velocities, which could explain the presence of multiple waterborne arrivals. The frequency composition of the secondary waves may also be explained by the fact that bending waves in thin shells are generally subsonic at low frequency and only radiate sound at higher frequencies (i.e., above the coincidence frequency[25]). It is also interesting to note that the fluid loading on the pipe is discontinuous at the air–water interface (near where the secondary waves appear to originate) and even subsonic bending waves radiate at discontinuities. The lack of up-going secondary waves in the data also suggests that bending waves, if present, are strongly damped in the wetted part of the pipe. This is consistent with the observation that they only radiate sound near the sea-surface. Nonetheless, it remains a subject for future investigation to confirm whether these high-frequency arrivals are indeed caused by bending waves in the pipe or whether some other mechanism is responsible.

C. Comparisons with other measurements

Sound levels at 10 m range from the conductor driving (see Fig. 9) were within the range of previously reported sound levels from impact driving of 0.61–0.76 m (24–30 in.) diameter steel pipe piles in much shallower water.[26,27] Measurements at 10 m from construction projects in California and Washington states, in water depths less than 15 m, reported per-pulse SEL in the range 173–187 dB re 1 μPa^{2}s (unmitigated). This suggests that deep-water conductor driving generates similar sound pressures to shallow water pile driving near the source, although the vertical extent of the source (and thus the ensonified area) is substantially greater. The fact that such comparisons are possible also underscores the benefit of reporting noise measurements at standard ranges—10 m has become a *de facto* standard range for reporting underwater piling noise studies in the western U.S. and Canada.[28,29]

A review of the literature found two prior studies that measured underwater noise generated by conductor driving. One study, by Jiang *et al.*, measured noise from offshore conductor driving at 0.75–2 km range from an oil platform in

the North Sea in 48 m of water.[30] Jiang *et al*. reported per-pulse 1/3-octave band SEL values that were similar in magnitude to the current study, but their data showed two frequency peaks—a low-frequency peak at 200 Hz and a high-frequency peak at 1250 Hz. The investigators could not determine the reason for the dual peak in the pulse spectrum, as information regarding the source was limited.[33] Jiang *et al*. did not report the dimensions of the conductor casing or hammer type, so it is unknown if they were similar to the current study. Another prior study measured underwater noise from land-based conductor driving at an oil production island.[31] As expected, land-based conductor driving generated much lower sound levels than were measured during the current study.

One unexpected result from the current study was that broadband sound levels from conductor driving were mostly steady over time, despite hammer energy doubling over the course of the operation. Previous measurements at an offshore wind farm reported a strong linear relationship (~6 dB peak increase per doubling of hammer energy) between radiated sound pressure and hammer energy.[32] The reason for this apparent inconsistency is unclear, although the wind farm measurements used a much larger hammer, and sampled a much larger range of hammer energy settings (80–800 kJ). In the current study, variability in other factors, such as the decreasing magnitude of the toe reflection, could have obscured the relationship between hammer energy and radiated sound level.

VI. CONCLUSIONS

Beamforming measurements of underwater noise from impact driving of conductor casings at a deep-water platform confirmed that low-frequency (<1 kHz) sound energy was clearly associated with Mach wave radiation (17.6° grazing angle) distributed over the water column. The strong downward directivity of the source, combined with the soft seabed at the measurement site, resulted in a shadow zone near the sea-surface in which broadband received levels were 10–15 dB lower than inside the Mach cone. Beamforming analysis of seabed refracted waves confirmed that the seabed at the measurement site was acoustically soft (critical angle <9°), which likely contributed to the lower sound levels measured in the shadow zone. This finding indicates that receivers outside the Mach cone may be exposed to much lower broadband sound levels, which is important to consider when assessing impacts of noise on marine organisms near deep-water pile driving.

Beamforming measurements also showed that the conductor driving generated secondary high-angle (>45° grazing) wave arrivals, which originated near the sea-surface, and which were delayed with respect to the Mach waves. These secondary waves were the dominant contributor to the high-frequency (>1 kHz) sound spectrum of the noise. Back-propagation of 1/3-octave band levels from multiple hydrophones confirmed that low frequencies decayed according to conical wave spreading, whereas high frequencies decayed according to spherical wave spreading. Taken together, these observations strongly suggested the existence of two separate sound generation mechanisms for low- and high-frequency sounds from impact driving of the steel pipe. The contribution of these secondary waves from conductor driving to the noise field might be particularly important in light of recently introduced weighting schemes that emphasize frequencies above 1 kHz for mid- and high-frequency cetaceans.[1,5]

Sound level data collected during this study could help future assessments that address the effects of deep-water pile driving operations on marine organisms. Source level measurements from this study could also be used to validate structural acoustic models that seek to reproduce the detailed noise field from impact pile driving operations. This study found that sound levels 10 m from deep-water conductor driving were within the range of those reported for shallow water pile driving. Thus, the physical mechanism responsible for generating high-frequency noise may be the same as well—this is a possible topic for future investigation.

ACKNOWLEDGMENTS

The field work for this study was carried out by A.M. and Robert Mills (JASCO). Angela Schlesinger and Robert Mills (JASCO) assisted with the sound level analysis. Vessel support during deployment and retrieval of the moorings was provided by Capt. Danny Castagnola (M/V *Danny C*), Steve Webster (Aqueos Corp., Ventura, CA) and their respective team members. Aaron Ochs, Bryan Chapman, and Darrel Landry (ExxonMobil, Houston, TX) provided logistical support during the measurement program. Michael Strickland (ExxonMobil) provided logs of hammer energy and conductor penetration. Katherine Williams and Roberto Racca (JASCO) and Mike Jenkerson and Changyong Zhang (ExxonMobil) provided editorial feedback during preparation of the draft manuscript. Two anonymous reviewers also provided several suggestions for improving the original manuscript. This work was funded by ExxonMobil.

[1]B. L. Southall, A. E. Bowles, W. T. Ellison, J. J. Finneran, R. L. Gentry, C. R. Greene, Jr., D. Kastak, D. R. Ketten, J. H. Miller, P. E. Nachtigall, W. J. Richardson, J. A. Thomas, and P. L. Tyack., "Marine mammal noise exposure criteria: Initial scientific recommendations," Aquat. Mamm. **33**(4), 411–521 (2007).

[2]P. G. Reinhall and P. H. Dahl, "Underwater Mach wave radiation from impact pile driving: Theory and observation," J. Acoust. Soc. Am. **130**(3), 1209–1216 (2011).

[3]M. B. Halvorsen, B. M. Casper, C. M. Woodley, T. J. Carlson, and A. N. Popper, "Threshold for onset of injury in Chinook salmon from exposure to impulsive pile driving sounds," PLoS One **7**(6), e38968 (2012).

[4]A. N. Popper, A. D. Hawkins, R. R. Fay, D. A. Mann, S. Bartol, T. J. Carlson, S. Coombs, W. T. Ellison, R. L. Gentry, M. B. Halvorsen, S. Løkkeborg, P. H. Rogers, B. L. Southall, D. G. Zeddies, and W. N. Tavolga, "Sound exposure guidelines for fishes and sea turtles: A technical report prepared by ANSI-Accredited Standards Committee S3/SC1 and registered with ANSI," SpringerBriefs in Oceanography, Vol. ASA S3/SC1.4 TR-2014, American Standards Association, New York, 2014.

[5]National Marine Fisheries Service, "Technical guidance for assessing the effects of anthropogenic sound on marine mammal hearing: Underwater acoustic thresholds for onset of permanent and temporary threshold shifts," NOAA Technical Memorandum NMFS-OPR-55, U.S. Department of Commerce, NOAA, 2016, pp. 1–178.

[6]A. MacGillivray and R. Racca, "Sound pressure and particle velocity measurements from marine pile driving at Eagle Harbor Maintenance Facility,

Bainbridge Island WA," Technical Report prepared by JASCO Research Ltd. for Washington State Department of Transportation, 2005, pp. 1–13.
[7]J. A. Reyff, "Underwater sound levels associated with construction of the Benicia-Martinez Bridge, acoustical evaluation of an unconfined air-bubble curtain system at Pier 13," Document No. 25, Technical Report, California Department of Transportation (Illingworth and Rodkin, Inc., Petaluma, CA), 2003.
[8]C. Erbe, "Underwater noise from pile driving in Moreton Bay, Qld," Acoust. Austral. **37**(3), 87–92 (2009).
[9]P. T. Madsen, M. Wahlberg, J. Tougaard, K. Lucke, and P. L. Tyack, "Wind turbine underwater noise and marine mammals: Implications of current knowledge and data needs," Mar. Ecol. Prog. Ser. **309**, 279–295 (2006).
[10]H. Bailey, B. Senior, D. Simmons, J. Rusin, G. Picken, and P. M. Thompson, "Assessing underwater noise levels during pile-driving at an offshore windfarm and its potential effects on marine mammals," Mar. Pollut. Bull. **60**(6), 888–897 (2010).
[11]P. H. Dahl and P. G. Reinhall, "Beam forming of the underwater sound field from impact pile driving," J. Acoust. Soc. Am. **134**(1), EL1–EL6 (2013).
[12]J. V. Carretta, E. Oleson, D. W. Weller, A. R. Lang, K. A. Forney, J. R. Baker, B. Hanson, K. Martien, M. M. Muto, T. Orr, H. Huber, M. S. Lowry, J. Barlow, D. Lynch, L. Carswell, R. L. J. Brownell, and D. K. Mattila, "Draft U.S. Pacific Marine Mammal Stock Assessments," 2013, pp. 1–311.
[13]American Petroleum Institute, "API Spec 5L, 44th edition: Specification for line pipe" (API Publishing Services, Washington, DC, 2008).
[14]P. T. Madsen, "Marine mammals and noise: Problems with root mean square sound pressure levels for transients," J. Acoust. Soc. Am. **117**(6), 3952–3957 (2005).
[15]V. Kandia and Y. Stylianou, "Detection of sperm whale clicks based on the Teager-Kaiser energy operator," Appl. Acoust. **67**, 1144–1163 (2006).
[16]A. V. Oppenheim and R. W. Schafer, *Discrete-Time Signal Processing*, 2nd ed. (Prentice-Hall, Englewood Cliffs, NJ, 1999), pp. 1–870.
[17]J. A. Nelder and R. Mead, "A simplex method for function minimization," Comp. J. **7**(4), 308–313 (1965).
[18]E. L. Hamilton, "Geoacoustic modeling of the sea floor," J. Acoust. Soc. Am. **68**(5), 1313–1340 (1980).
[19]International Ocean Discovery Program, "Ocean Drilling Data—Leg 146, Site 893," Janus data, Exp 1-312 (2013), available at http://iodp. tamu.edu/janusweb/general/dbtable.cgi?leg=146&site=893 (Last viewed Feb. 2014).
[20]J. A. Reid, *Point Coverage SCASMPL: Sediment sample data for the Channel Islands and Santa Barbara Channel Region* (U.S. Geological Survey, Santa Cruz, CA, 2005).
[21]I. L. Vér and L. L. Beranek (eds.), *Noise and vibration control engineering: Principles and applications*, 2nd ed. (Wiley, New York, 2005), pp. 1–976.
[22]J. J. Finneran and C. E. Schlundt, "Effects of fatiguing tone frequency on temporary threshold shift in bottlenose dolphins (*Tursiops truncatus*)," J. Acoust. Soc. Am. **133**(3), 1819–1826 (2013).
[23]R. A. Kastelein, R. Gransier, M. A. T. Marijt, and L. Hoek, "Hearing frequency thresholds of harbor porpoises (*Phocoena phocoena*) temporarily affected by played back offshore pile driving sounds," J. Acoust. Soc. Am. **137**(2), 556–564 (2015).
[24]A. W. Leissa, *Vibration of Shells* (National Aeronautics and Space Administration, Washington, D.C., 1973), pp. 1–438.
[25]S. A. Hambric and J. B. Fahnline, "Structural acoustics tutorial—Part 2: Sound—Structure interaction," Acoust. Today **3**(2), 9–27 (2007).
[26]J. Laughlin, "Underwater sound levels associated with restoration of the Friday Harbor ferry terminal," Washington Department of Transportation, Seattle, Washington, 2005, pp. 1–130.
[27]Illingworth and Rodkin, Inc., "Appendix I. Compendium of pile driving sound data," in *Technical Guidance for Assessment and Mitigation of the Hydroacoustic Effects of Pile Driving on Fish* (California Department of Transportation, Sacramento, CA, 2007), p. 129.
[28]ICF Jones and Stokes, and Illingworth and Rodkin, Inc., "Technical guidance for assessment and mitigation of the hydroacoustic effects of pile driving on fish," California Department of Transportation (CALTRANS), Sacramento, CA, 2009, pp. 1–298.
[29]Washington State Department of Transportation, "Advanced training manual: Biological assessment preparation for transportation projects," Technical Report, Washington State Department of Transportation Environmental Services (2013), Vol. 02-2013, pp. 1–93.
[30]J. Jiang, V. L. G. Todd, J. Gardiner, and I. B. Todd, "Measurements of underwater conductor hammering noise: Compliance with the German UBA limit and relevance to the harbour porpoise (*Phocoena phocoena*)," in *EuroNoise 2015*, Maastrich, Netherlands (2015), pp. 1369–1374.
[31]S. B. Blackwell, J. W. Lawson, and M. T. Williams, "Tolerance by ringed seals (*Phoca hispida*) to impact pipe-driving and construction sounds at an oil production island," J. Acoust. Soc. Am. **115**(5), 2346–2357 (2004).
[32]S. P. Robinson, P. A. Lepper, and J. Ablitt, "The measurement of the underwater radiated noise from marine piling including characterisation of a 'soft start' period," in *Oceans 2007-Europe* IEEE, Aberdeen, UK (18–21 June 2007), pp. 1–6.
[33]J. Jiang (personal communication, 2016).